Response of Laminated Composite Flat Panels to Sonic Boom and Explosive Blast Loadings

L. Librescu* and A. Nosier†
Department of Engineering Science and Mechanics
Virginia Polytechnic Institute and State University, Blacksburg, Virginia

This paper deals with a theoretical analysis of the dynamic response of shear deformable symmetrically laminated rectangular composite flat panels exposed to sonic boom and explosive blast loadings. The pertinent governing equations incorporating transverse shear deformation, transverse normal stress, as well as the higher-order effects are solved by using the integral-transform technique. The obtained results are compared with their counterparts obtained within the framework of the first-order transverse shear deformation and the classical plate theories and some conclusions concerning their range of applicability are outlined. The paper also contains a detailed analysis of the influence played by the various parameters characterizing the considered pressure pulses as well as the material and geometry of the plate.

I. Introduction

THE response of elastic structures to time-dependent pulses, such as sonic boom and blast loadings, constitutes a subject that is currently of much interest in the design of aeronautical and space vehicles as well as of marine and terrestrial ones. With very few exceptions, its study was done in the past for the case of thin isotropic structural members (see e.g. Refs. 1–8).

With the advent of the new composite material structures and their increased use in the aerospace industry, there is a need to reconsider the problem of structural response. This is due to the fact that the new composite material structures exhibit distinguishing features as compared to their metallic counterparts. The former ones are characterized by a weak rigidity in transverse shear and by high degrees of orthotropy of the layer materials; the latter ones are constituted of isotropic materials and may be considered to exhibit an infinite rigidity in transverse shear. That is why, in order to get correct results for the response behavior of flat structures made of advanced composite materials, refined plate models have to be used. They should incorporate transverse shear deformation and transverse normal stress effects and should account for the higher-order effects. The analytical studies devoted to the dynamic response of shear deformable laminated and single layered flat panels to blast loadings are very few. In this sense, the reader is referred to Refs. 9, 10, and 11, respectively. Within this paper, the far-field overpressure produced by an aircraft flying supersonically in the Earth's atmosphere (referred to as the sonic-boom pressure pulse) or by any supersonic projectile, rocket, or missile as well as the one resulting from an explosive blast (see Refs. 3 and 5–10) are considered to predict the panel response. The time history of the sonic boom is described as an N-shaped pulse, whose negative phase duration is included as a variable in the analysis. As concerns the explosive blast, its time history is approximated both as an exponentially decaying pressure pulse and, in an approximated way, by a triangular pulse. The results obtained within a higher-order plate theory (HSDT) are compared with their first-order transverse shear deformation (FSDT) and classical (CLT) counterparts, and some conclusions concerning their range of applicability are outlined. In addition, the obtained numerical results allow one to draw conclusions about the influence played by the various physical and geometrical parameters entering the problem. Having in view that the severity of the dynamic response can be conveniently measured in terms of the dynamic magnification factor (DMT), its variation for several pulse shapes is also displayed in the paper.

II. Governing Equations

The response analysis will be performed within the framework of a higher-order bending theory of cross-ply symmetrically laminated composite plates. Previously formulated in Refs. 13 and 14, this theory exhibits all the advantages embodied in its FSDT counterpart both with regards to the number of involved unknown quantities and the order of the associated governing equations. However, in contrast to FSDT, the present theory is based on 1) a parabolic representation of transverse shear-stress components across the plate thickness (thus avoiding the need for a shear correction factor) and 2) the elimination of the contradictory assumptions involving the simultaneous consideration of zero transverse normal stress σ_{33} and zero transverse normal strain e_{33}. Furthermore, the results predicted by HSDT will be compared with the ones obtained within the framework of FSDT and CLT. By adopting the assumptions formulated in Ref. 13 and by referring the points of the midplane of the laminated composite rectangular ($a \times b$) plate to a Cartesian system of coordinates x-y parallel at each point with the principal material directions, the governing equations (see Ref. 13) may be reduced to

$$
\begin{aligned}
&a_1 w_{,xxx} + a_2 w_{,xyy} + a_3 \psi_{x,xx} + a_4 \psi_{x,yy} + a_5 \psi_{y,xy} \\
&\quad + a_6 \psi_x + a_7 w_{,x} = a_8 \ddot{\psi}_x + a_9 \ddot{w}_{,x} \\
&b_1 w_{,yyy} + b_2 w_{,yxx} + b_3 \psi_{y,yy} + b_4 \psi_{y,xx} + b_5 \psi_{x,xy} \\
&\quad + b_6 \psi_y + b_7 w_{,y} = b_8 \ddot{\psi}_y + b_9 \ddot{w}_{,y} \\
&c_1 \psi_{x,x} + c_2 \psi_{y,y} + c_3 w_{,xx} + c_4 w_{,yy} + c_5 P_z = c_6 \ddot{w}
\end{aligned} \tag{1}
$$

The FSDT counterparts of Eqs. (1) are given by (see e.g., Ref. 13)

$$
\begin{aligned}
&a_3 \psi_{x,xx} + a_4 \psi_{x,yy} + a_5 \psi_{y,xy} + a_6 \psi_x + a_7 w_{,x} = a_8 \ddot{\psi}_x \\
&b_3 \psi_{y,yy} + b_4 \psi_{y,xx} + b_5 \psi_{x,yx} + b_6 \psi_y + b_7 w_{,y} = b_8 \ddot{\psi}_y \\
&c_1 \psi_{x,x} + c_2 \psi_{y,y} + c_3 w_{,xx} + c_4 w_{,yy} + c_5 P_z = c_6 \ddot{w}
\end{aligned} \tag{2}
$$

Received Jan. 23, 1989; revision received June 9, 1989.

*Professor.

†Graduate Research Associate.

where, in contrast with HSDT, the higher-order effects as well as the one played by σ_{33} are disregarded. The coefficients appearing in Eqs. (1) and (2), which are functions of stiffness quantities, are displayed in Appendix A. In particular, the coefficients c_3 and c_4 include the effect of the in-plane edge loads T_{11} and T_{22}, respectively, which play a substantial role in the response behavior. The structural response corresponding to CLT can be obtained as a special case from FSDT by considering the transverse shear moduli to be infinite quantities. For convenience, in Eqs. (1) and (2), the notations w, ψ_x, and ψ_y replace

$$\overset{(0)}{v_3},\ \overset{(1)}{v_1},\ \text{and}\ \overset{(1)}{v_2}$$

respectively, originally introduced in Ref. 13. Here, w denotes the transverse displacement and ψ_x and ψ_y denote the rotations of the normals about the y- and x-axes, respectively. Associated with Eqs. (1), the boundary conditions for a simply supported plate are (see Ref. 13)

$$\psi_y = 0,\ w = 0,\ \text{and}\ a_1 w_{,xx} + a_3 \psi_{x,x} = 0 \ \text{at}\ x = 0,\ a \tag{3a}$$

and

$$\psi_x = 0,\ w = 0,\ \text{and}\ b_1 w_{,yy} + b_3 \psi_{y,y} = 0 \ \text{at}\ y = 0,\ b \tag{3b}$$

and the initial conditions are prescribed to be

$$\psi_x(x,y,0) = \tilde{\psi}_x(x,y),\ \psi_y(x,y,0) = \psi_y(x,y),\ w(x,y,0) = \tilde{w}(x,y),\ w_{,x}(x,,y,0) = \tilde{w}_x(x,y),\ w_{,y}(x,y,0) = \tilde{w}_y(x,y),\ \dot{\psi}_x(x,y,0) = \tilde{\dot{\psi}}_x(x,y)\ \dot{\psi}_y(x,y,0) = \tilde{\dot{\psi}}_y(x,y),\ \dot{w}(x,y,0) = \tilde{\dot{w}}(x,y),\ \dot{w}_{,x}(x,y,0) = \tilde{\dot{w}}_x(x,y)\ \dot{w}_{,y}(x,y,0) = \tilde{\dot{w}}_y(x,y) \tag{4}$$

Here the single and double over tildes denote prescribed quantities for the basic variables ψ_x, ψ_y, w as well as for $w_{,x}$ and $w_{,y}$ and their time derivatives, respectively, at $t = 0$.

As concerns the boundary conditions associated with FSDT, they are

$$\psi_y = 0,\ w = 0,\ \text{and}\ \psi_{x,x} = 0 \ \text{at}\ x = 0,a \tag{5a}$$

and

$$\psi_x = 0,\ w = 0,\ \text{and}\ \psi_{y,y} = 0 \ \text{at}\ y = 0,b \tag{5b}$$

III. Solution Procedure

The integral-transform technique will be used to solve the dynamic-response problem. To this end, Eqs. (1) are subjected to a Laplace transform with respect to time and successively $(1)_1$, $(1)_2$, and $(1)_3$ to finite Fourier cosine-sine, sine-cosine, and sine-sine transforms, respectively. Appropriate use of initial and boundary conditions given by Eqs. (3) and (4) yields an algebraic system of equations expressed in the transformed space as

$$\begin{bmatrix} (K_{11} + a_8 s^2) & K_{12} & (K_{13} + a_9 \alpha_m s^2) \\ K_{21} & (K_{22} + b_8 s^2) & (K_{23} + b_9 \beta_n s^2) \\ K_{31} & K_{32} & (K_{33} + c_6 s^2) \end{bmatrix} \begin{Bmatrix} \overset{(cs)}{\bar{\psi}_x}(m,n,s) \\ \overset{(sc)}{\bar{\psi}_y}(m,n,s) \\ \overset{(ss)}{\bar{w}}(m,n,s) \end{Bmatrix} = \begin{Bmatrix} \bar{T}_1 \\ \bar{T}_2 \\ \bar{T}_3 \end{Bmatrix} \tag{6}$$

The terms K_{ij} and $\bar{T}_i$ are given in Appendix B.

In addition, $\alpha_m = m\pi/a$ and $\beta_n = n\pi/b$; m and n denote Fourier transform variables associated with x and y, respectively, and s denotes Laplace transform variable associated with the time variable t. An overbar accompaying a quantity identifies its Laplace transform [that is $L\{a(t)\} = \bar{a}(s)$], and $(.)^{(s)}$ and $(.)^{(c)}$ denote finite sine and cosine Fourier transforms, respectively. It should be remarked that the right side of Eqs. (6) contains the initial conditions as part of the forcing function.

Starting with the system of Eqs. (6), the dynamic response and its associated eigenfrequency problem could be analyzed. For the dynamic response problem, employment in Eqs. (6) of Cramer's rule and partial fraction expansion technique yields $\bar{\psi}_x^{(cs)}$, $\bar{\psi}_y^{(sc)}$ and $\bar{w}^{(ss)}$ as

$$\overset{(cs)}{\bar{\psi}_x}(m,n,s) = \sum_{j=1}^{3} \bar{H}_{1j}(m,n,s)\ \bar{T}_j;\ \overset{(sc)}{\bar{\psi}_y}(m,n,s) = \sum_{j=1}^{3} \bar{H}_{2j}(m,n,s)\ \bar{T}_j\ \overset{(ss)}{\bar{w}}(m,n,s) = \sum_{j=1}^{3} \bar{H}_{3j}(m,n,s)\ \bar{T}_j \tag{7}$$

where

$$\bar{H}_{ij}(m,n,s) = \frac{1}{\lambda_1} \sum_{k=1}^{3} \frac{A_{ijk}}{(s^2 + \omega_k^2)} \tag{8}$$

Furthermore, in Eq. (8), A_{ijk} are expressed as

$$A_{ijk} = \frac{1}{\delta_k} \sum_{\ell=1}^{3} I_{ij\ell}\ \omega_k^{6-2\ell},\ (i,j,k = 1,2,3) \tag{9}$$

where

$$\delta_k (\equiv \delta_k^{(m,n)}) = (\omega_k^2 - \omega_m^2)(\omega_k^2 - \omega_n^2),\ (k \neq m \neq n),\ (k,m,n = 1,2,3,\ \textstyle\sum_k') \tag{10}$$

and $I_{ij\ell}$ are displayed in Appendix C. In Eqs. (10-12), ω_i^2 $(\equiv -s_i^2)$ represent the eigenfrequencies of the system obtained by setting the determinant of the coefficient matrix in Eqs. (6) equal to zero. By following this procedure, a cubic polynomial in $\Omega (\equiv \omega^2)$ is obtained

$$\lambda_1 \Omega^3 - \lambda_2 \Omega^2 + \lambda_3 \Omega - \lambda_4 = 0 \tag{11}$$

where the coefficients λ_i are given in Appendix C.

It appears evident that three eigenfrequencies, Ωi the roots of the characteristics Eq. (11), can be obtained for each pair of m and n. The inverse Laplace transform applied to Eqs. (7) yields the response quantities in the time domain as

$$\psi_x^{(cs)}(m,n,t) = M_{11}^{(cs)} L_{11}(m,n,t) + M_{12}^{(cs)} H_{11}(m,n,t) + M_{21}^{(sc)} L_{12}(m,n,t) + M_{22}^{(sc)} H_{12}(m,n,t) + M_{31}^{(ss)} L_{13}(m,n,t) + M_{32}^{(ss)} H_{13}(m,n,t) + \int_0^t H_{13}(m,n,t-\tau)\ P_z^{(ss)}(m,n,\tau)\ d\tau \tag{12a}$$

$$\psi_y^{(sc)}(m,n,t) = M_{11}^{(cs)}L_{21}(m,n,t) + M_{12}^{(cs)}H_{21}(m,n,t) + M_{21}^{(sc)}L_{22}(m,n,t) + M_{22}^{(sc)}H_{22}(m,n,t) + M_{31}^{(ss)}L_{23}(m,n,t) + M_{32}^{(ss)}H_{23}(m,n,t) + \int_0^t H_{23}(m,n,t-\tau)\, P_z^{(ss)}(m,n,\tau)\, d\tau \tag{12b}$$

$$w^{(ss)}(m,n,t) = M_{11}^{(cs)}L_{31}(m,n,t) + M_{12}^{(cs)}H_{31}(m,n,t) + M_{21}^{(sc)}L_{32}(m,n,t) + M_{22}^{(sc)}H_{32}(m,n,t) + M_{31}^{(ss)}L_{33}(m,n,t) + M_{32}^{(ss)}H_{33}(m,n,t) + \int_0^t H_{33}(m,n,t-\tau)\, P_z^{(ss)}(m,n,\tau)\, d\tau \tag{12c}$$

where

$$H_{ij}(m,n,t) \equiv L^{-1}\{\bar{H}_{ij}(m,n,s)\} = \frac{1}{\lambda_1}\sum_{k=1}^{3} A_{ijk}\frac{\sin}{\omega_k t}\omega_k \tag{13a}$$

$$L_{ij}(m,n,t) \equiv L^{-1}\{s\bar{H}_{ij}(m,n,s)\} = \frac{1}{\lambda_1}\sum_{k=1}^{3} A_{ijk}\cos\omega_k t \quad (i,j = 1,2,3) \tag{13b}$$

and

$$P_z^{(ss)}(m,n,t) \equiv L^{-1}\{\bar{P}_z^{(ss)}(m,n,s)\} \tag{13c}$$

For zero-initial conditions, Eqs. (12) reduce to

$$\psi_x^{(cs)}(m,n,t) = \int_0^t H_{13}(m,n,t-\tau)\, P_z^{(ss)}(m,n,\tau)\, d\tau \tag{14a}$$

$$\psi_y^{(sc)}(m,n,t) = \int_0^t H_{23}(m,n,t-\tau)\, P_z^{(ss)}(m,n,\tau)\, d\tau \tag{14b}$$

$$w^{(ss)}(m,n,t) = \int_0^t H_{33}(m,n,t-\tau)\, P_z^{(ss)}(m,n,\tau)\, d\tau \tag{14c}$$

where τ denotes a dummy-time variable. Successive application of inverse sine and cosine Fourier transforms to Eqs. (12) or (14) yields the primary response quantities in the physical space expressed as

$$\psi_x(x,y,t) = \frac{1}{a}\psi_x^{(c)}(0,y,t) + \frac{4}{ab}\sum_{m=1}^{\infty}\sum_{n=1}^{\infty}\psi_y^{(cs)}(m,n,t) \sin\beta_n y \cos\alpha_m x \tag{15a}$$

$$\psi_y(x,y,t) = \frac{2}{a}\sum_{m=1}^{\infty}\left[\frac{1}{b}\psi_y^{(sc)}(m,0,t) + \frac{2}{b}\sum_{n=1}^{\infty}\psi_y^{(sc)}(m,n,t)\right] \cos\beta_n y \sin\alpha_m x \tag{15b}$$

$$w(x,y,t) = \frac{4}{ab}\sum_{m=1}^{\infty}\sum_{n=1}^{\infty} w^{(ss)}(m,n,t)\sin\beta_n y \sin\alpha_m x \tag{15c}$$

where

$$\psi_x^{(c)}(m,y,t) = \frac{2}{b}\sum_{n=1}^{\infty}\psi_x^{(cs)}(m,n,t)\sin\beta_n y \tag{16}$$

In Eqs. (15) and (16), $\psi_x^{(cs)}$, $\psi_y^{(sc)}$ and $w^{(ss)}$ are given by Eqs. (12) or (14) depending on whether the initial conditions are nonzero or zero, respectively. It should be mentioned that the response quantities as expressed by Eqs. (15) correspond to a transverse load $P_z(x,y,t)$ exhibiting an arbitrary spatial and time dependence. This means that the above results could be applied to determine the structural response of cross-ply rectangular laminated plates to any type of pulse loadings. However, our concern will be confined to the cases of sonic boom and blast loadings only. In addition, it should be mentioned that the results obtained remain valid also for FSDT. In such a case, the proper expressions of the coefficients appearing in Eqs. (2) (Appendix A) will have to be used.

IV. Response to Blast and Sonic Boom-Type Loadings

Within the present paper, the response of composite float panels to explosive blast and sonic boom-type loadings will be studied. Due to their structural damaging effects, these types of loadings have been estimated by using both theoretical and experimental considerations. For the case of blast type loadings, various analytical expressions have been proposed and discussed in the literature (see e.g., Refs. 5 and 9 and also Ref. 10). As it was clearly established, the blast wave reaches the peak value in such a short time that the structure can be assumed to be loaded instantly. Due to the relative small dimensions of the plate when compared to the blast (and sonic boom) wave front it may also be assumed that the pressure is uniformly distributed over the plate. The overpressure-time history can be described in terms of the modified Friedlander exponential decay equation (see Refs. 7 and 8)

$$P_z(x,y,t)(\equiv P_z(t)) = P_m\left(1 - \frac{t}{t_p}\right)e^{-a't/t_p} \tag{17}$$

where the negative phase of the blast is included. In Eq. (19), P_m denotes the peak reflected pressure in excess of the ambient one; t_p denotes the positive phase duration of the pulse measured from the time of arrival of the blast at the plate surface; and a' denotes a decay parameter which has to be adjusted to approximate the pressure curve from the blast test. A depiction of the ratio P_z/P_m vs time for various values of the ratio a'/t_p and fixed value of t_p is displayed in Fig. 1. As it could be inferred, the triangular load may be viewed as a limiting case of Eq. (19), that is for $a'/t_p \to 0$. As concerns the sonic boom loadings, they could be modeled as an N-shaped pressure pulse. Such a pulse corresponds to an idealized far-field sonic boom disturbance arriving at a normal incidence. The pressure time history of the N-wave shock pulse experienced by the

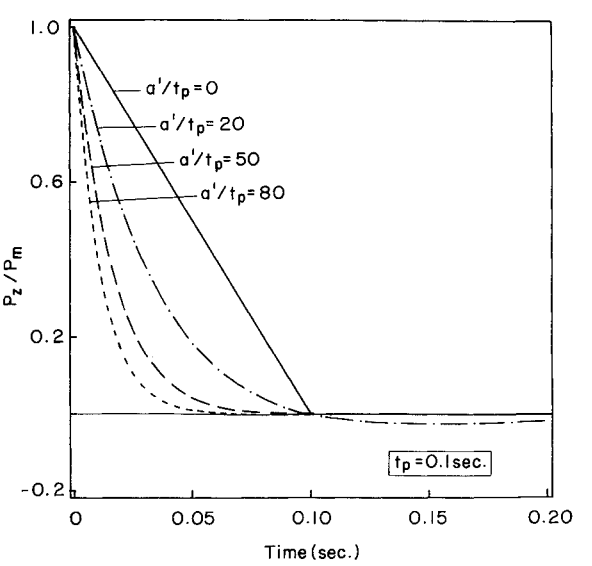

Fig. 1 Typical variation of blast overpressure with respect to time.

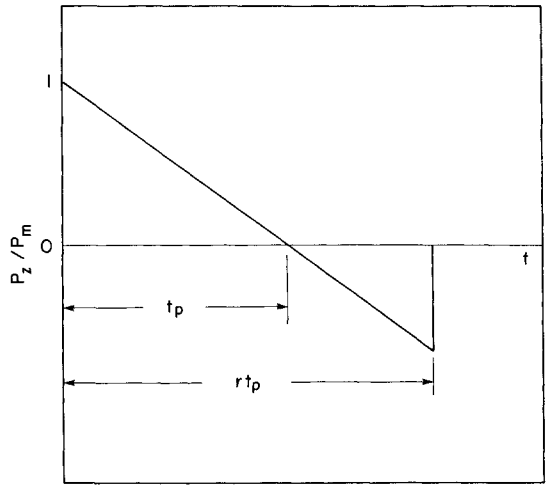

Fig. 2 Typical pressure time-history associated with an asymmetric N-shaped pulse.

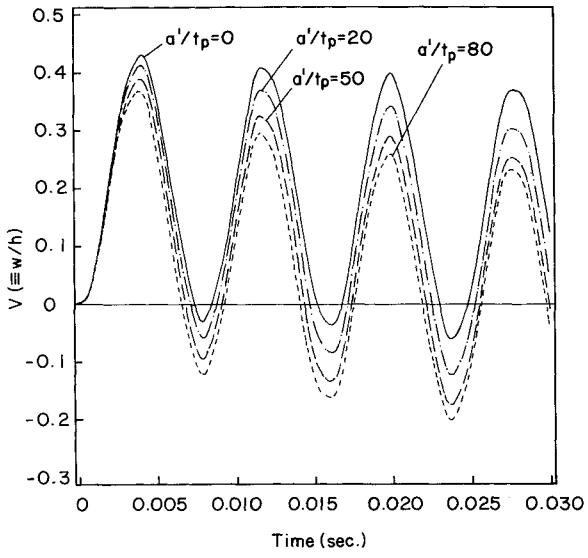

Fig. 3 Time history of the nondimensional deflection response of the center of a three-layered square plate (Structure I) characterized by $a/h = 15$, $a = 100$ in. to a normal blast loading characterized by various a' and $t_p = 0.1$ s (the results are obtained within HSDT with $p_m = 500$ psi).

plate may be described by Refs 2-4 and 12.

$$P_z(x,y,t)(\equiv P_z(t)) = \begin{cases} P_m\left(1 - \dfrac{t}{t_p}\right) & \text{for } 0 < t < rt_p \\ 0 & \text{for } t < 0 \text{ and } t > rt_p \end{cases} \tag{18}$$

where r denotes the shock pulse length factor, and P_m and t_p maintain the same meaning as in the case of blast loadings. It may easily be seen that 1) for $r = 1$, the N-shaped pulse degenerates into a triangular one; 2) for $r = 2$, a symmetric N-shaped pressure pulse is obtained; whereas 3) for $1 < r < 2$, the N-shaped pulse becomes an asymmetric one as shown in Fig. 2. In addition to the dynamic response for the transverse deflection, the dynamic magnification factor (DMF) will also be determined. The DMF is defined as the ratio of the maximum dynamic deflection to the static deflection at a point on the structure. The static deflection corresponds to a uniformly distributed loading of magnitude equal to the peak pressure of the pulse.

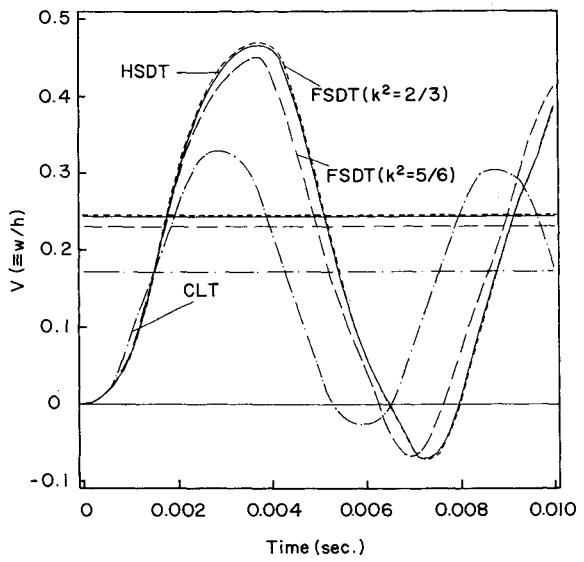

Fig. 4 Time history of the nondimensional deflection response of the center of a three-layered square plate (Structure II) ($a/h = 20$; $a = 100$ in.) to a blast loading characterized by $t_p = 0.1$ s, $a' = 1.98$ and $P_m = 400$ psi (the results are obtained within HSDT, FSDT and CLT. The horizontal lines correspond to the static deflection, allowing one to emphasize the dynamic overshoot of the response).

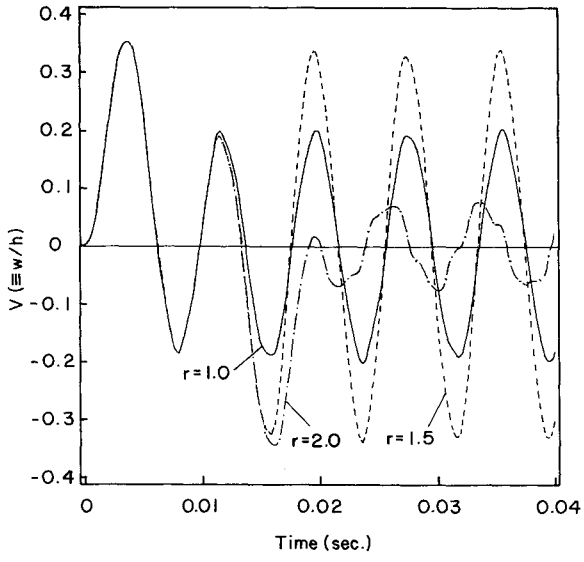

Fig. 5 Time history of the nondimensional deflection response of the center of a three-layered square plate (Structure I) ($a/h = 15$, $a = 100$ in.) to an N-shaped pulse characterized by various values of r and by $P_m = 500$ psi and $t_p = 0.01$ s (here HSDT was used only).

Two types of structures will be considered in the subsequent numerical illustrations. One of them, labeled "Structure I," is a three-layered cross ply (0-, 90-, and 0-deg) square plate whose midlayer is two times thicker than the external ones. Also it is assumed that the orthotropic material of all laminae is the same, its properties being given by

$$E_1 = 19.2 \times 10^6 \text{ psi}, \quad E_2 = 1.56 \times 10^6 \text{ psi}, \quad E_3 = 1.56 \times 10^6 \text{ psi}$$

$$G_{12} = 0.82 \times 10^6 \text{ psi}, \quad G_{13} = 0.82 \times 10^6 \text{ psi},$$

$$G_{23} = 0.523 \times 10^6 \text{ psi}, \quad \nu_{12} = 0.24, \quad \nu_{13} = 0.24, \quad \nu_{23} = 0.49$$

The second structure labeled "Structure II" is also a three-lay-

ered square plate, whose midlayer is two times thicker than the external ones. It is assumed that the material of the laminae is transversely isotropic, the plane of isotropy being parallel at each point to the midplane of the structure. It is further assumed that the material properties of the layers are given as

$$E_{(2)}/G'_{(2)} = 20;\ E_{(1)}/G'_{(1)}\ (\equiv E_{(3)}/G'_{(3)}) = 50;\ E_{(1)}/E'_{(1)}$$

$$(\equiv E_{(3)}/E'_{(3)}) = 5;\ E_{(2)}/E'_{(2)} = 2;\ E_{(1)}/E_{(2)} = E_{(3)}/E_{(2)} = 10;$$

$$\nu = {}_{(i)} = \nu'_{(i)} = 0.24,\ (i = 1,2,3)$$

For both structures, the material density for all layers is taken as $\rho = 13 \times 10^{-5}$ lb s^2/in.^{4} Here, the indices 1 and 3 area associated with the external layers and the index 2 with the midlayer; E and ν are the Young's modulus and Poisson's ratio, respectively, associated with the isotropy plane; and E', ν' and G' denote the Young's modulus, Poisson's ratio and transverse shear modulus, respectivley, in the planes normal to the isotropy plane. Figures 3 and 4 and Figs. 5–9 display the time history of the dimensionless plate center deflection for the case of the blast loading and of the N-shaped pulse, respectively, and Figs. 10 and 11 display the variation of DMF for the plate subjected to a triangular blast and to an N-shaped pulse, respectively. In all these calculations, the initial conditions were assumed to be zero.

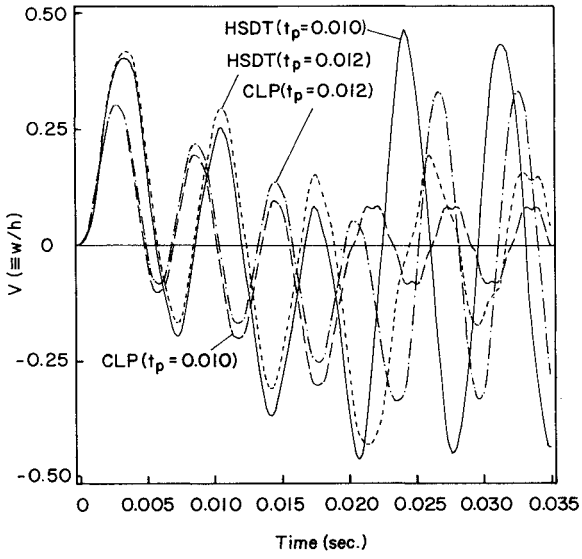

Fig. 6 Time history of the nondimensional deflection response of the center of a three-layered square plate (Structure II) ($a/h = 20$, $a = 100$ in.) to a symmetric N-pulse characterized by two different values of t_p and $P_m = 400$ psi (here HSDT and CLT are compared).

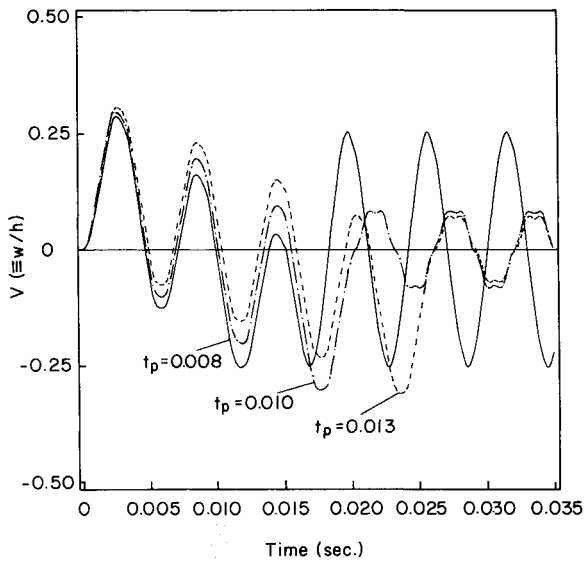

Fig. 7 Time history of the nondimensional deflection response of the center of a three-layered square plate (Structure II) ($a/h = 20$ $a = 100$ in.) to a symmetric N-pulse characterized by three different values of the t_p parameter and $P_m = 400$ psi (here the results are obtained within the framework of CLT, only).

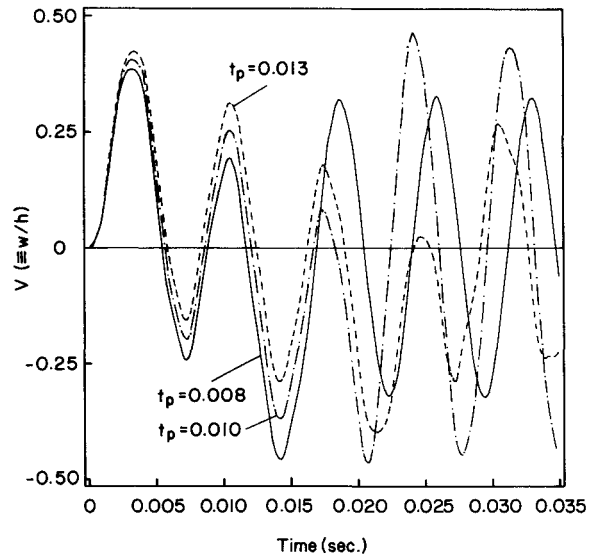

Fig. 8 Time history of the nondimensional deflection response of the center of a three-layered square plate (Structure II) having the same geometrical and pulse characteristics as the ones describing in Fig. 10 (here the results are obtained within the framework of HSDT).

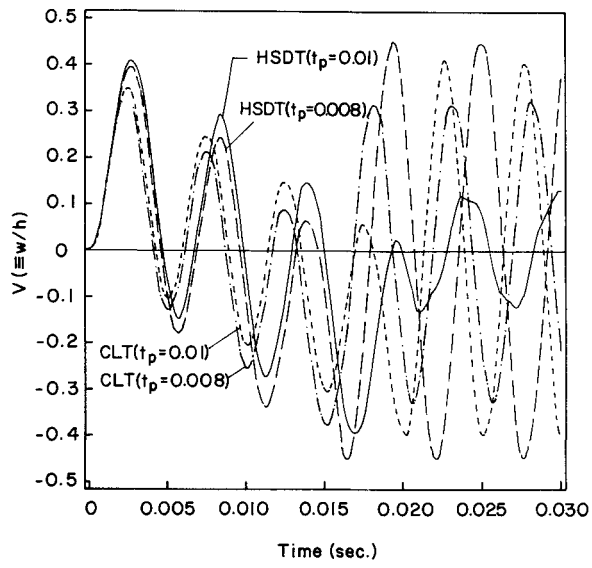

Fig. 9 Time history of the nondimensional deflection response of the center of a three-layered square plate (Structure I) ($a/h = 10$, $a = 100$ in.) subjected to a symmetric N-pulse characterized by two values of t_p and $P_m = 2500$ psi. Here the results are obtained within the framework of HSDT and CLT.

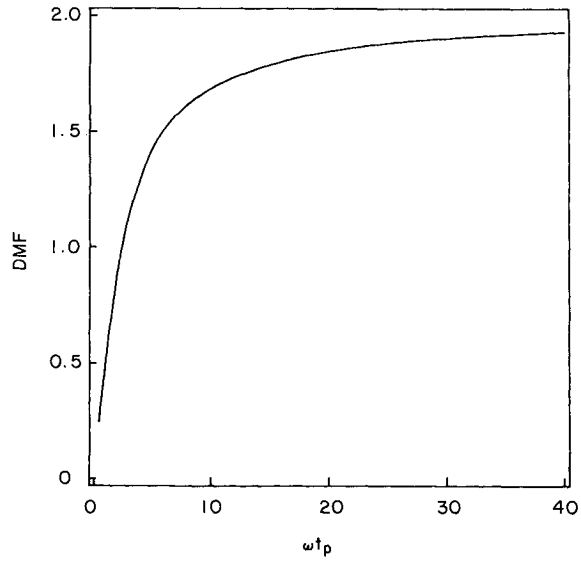

Fig. 10 Variation of dynamic magnification factor vs ωt_p for a square plate (Structure I), characterized by $a/h = 10$ and $a = 100$ in., and subjected to a triangular blast load (t_p represents the pulse length and ω the fundemental frequency predicted by HSDT).

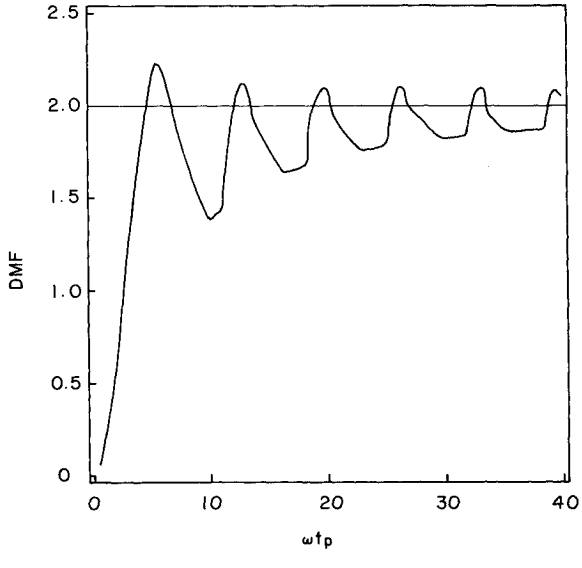

Fig. 11 Variation of dynamic amplification factor vs ωt_p for a square plate (Structure I) having the same geometrical characteristics as in Fig. 10 and subjected to a symmetric N-shaped pulse (t_p represents the posivite duration of the pulse and ω denotes the fundamental frequency predicted by HSDT).

V. Discussion and Conclusions

In Figs. 3 and 4, the dimensionless deflection $V(\equiv w/h)$ response of the center of a three-layered square plate to a normal blast loading is displayed. Fig. 3 shows that with the decrease of the parameter a', higher amplitudes of the deflection are obtained. Figure 4 compares the deflection response obtained within HSDT, FSDT (with two shear correction factors) and CLT. As it is evident from these plots (obtained for the Structure II), $K^2 = 2/3$ gives better results when compared with their counterpart obtained with $K^2 = 5/6$. Opposite results (which are not displayed here) are obtained when Structure I is considered. In this case, $K^2 = 5/6$ constitutes a better selection of the shear correction factor than $K^2 = 2/3$. This trend reveals once more the importance of approaching the response in the framework of a higher-order plate theory, which in contrast with FSDT does not require incorporation of such a correction factor, largely dependent on the lamination sequence, relative anisotropy of the layers, etc. Figures 5-9 display the deflection response of the center of a square plate to a sonic boom. Figure 5 reveals the quantitative and qualitative differences in the response deflections due to a symmetric ($r = 2$), asymmetric ($r = 1.5$) and a degenerated ($r = 1$) N-shaped pulse, and Fig. 6 reveals the strong influence played by the parameter t_p (that is by the duration of the positive phase of N-shaped pulse). This figure also shows that even in the case of nonthick plates (that is when $a/h = 20$), the results obtained within the framework of the classical theory are in total disagreement with the ones incorporating transverse shear deformation effects. Though during the positive phase of the pulse, the deflection response obtained as per the CLT follows the well known trend (in the sense that it is underestimated) within the negative phase of the pulse, it may result in higher values as compared to their shear deformable counterparts. However, for thin plates, the results (not displayed here) reveal that the response characteristics obtained within classical and shear deformable theories are in perfect agreement. Figures 7-9 reveal again the strong influence played by the parameter t_p principally within and after the negative phase of the pulse as well as the unreliable character of the results furnished by the CLT. Finally, Figs. 10 and 11 display the variation of DMF vs the nondimensional time ωt_p (where ω denotes the fundamental frequency predicted by HSDT). The pattern of variation of DMF for the case of a triangular blast and the N-shaped loadings, as revealed by these graphs, is similar to the one in Refs. 3 and 15 for the case of a metallic structure. It should be added that the results obtained in this paper could also be used to determine the time histories of ψ_x and ψ_y and, as a result, of strain and stress quantities in any point of the panel.

Acknowledgment

The partial support of this work by NASA Langley Research Center through Grant NAG-1-749 is gratefully acknowledged.

Appendix A: Rigidity and mass terms appearing in Equations 1 and 2

$$a_1 = -\frac{4}{3h^2} F_{11}^{11} - \delta_A (M_{11}^{11} - \frac{4}{3h^2} N_{11}^{11})$$

$$a_2 = -\frac{4}{3h^2} (F_{22}^{11} + 2F_{12}^{12}) - \delta_A (M_{22}^{11} - \frac{4}{3h^2} N_{22}^{11})$$

$$a_3 = D_{11}^{11} - \frac{4}{3h^2} F_{11}^{11} - \delta_A (M_{11}^{11} - \frac{4}{3h^2} N_{11}^{11})$$

$$a_4 = D_{12}^{12} - \frac{4}{3h^2} F_{12}^{12}$$

$$a_5 = D_{22}^{11} - \frac{4}{3h^2} F_{22}^{11} + D_{12}^{12} - \frac{4}{3h^2} F_{12}^{12} - \delta_A (M_{22}^{11} - \frac{4}{3h^2} N_{22}^{11})$$

$$a_6 = -R_{13}^{13} + \frac{4}{h^2} S_{13}^{13} = a_7$$

$$a_8 = \delta_c (m_3 - \frac{4}{3h^2} m_5)$$

$$a_9 = -\delta_A \delta_B I_{33}^{11} - \delta_c \frac{4}{3h^2} m_5$$

$$b_1 = -\frac{4}{3h^2} F_{22}^{22} - \delta_A M_{22}^{22} - \frac{4}{3h^2} N_{22}^{22})$$

$$b_2 = -\frac{4}{3h^2} (F_{11}^{22} + 2F_{21}^{21}) - \delta_A (M_{11}^{22} - \frac{4}{3h^2} N_{11}^{22})$$

$$b_3 = D_{22}^{22} - \frac{4}{3h^2} F_{22}^{22} - \delta_A (M_{22}^{22} - \frac{4}{3h^2} N_{22}^{22})$$

$$b_4 = D_{21}^{21} - \frac{4}{3h^2} F_{21}^{21}$$

$$b_5 = D_{11}^{22} - \frac{4}{3h^2} F_{11}^{22} + D_{21}^{21} - \frac{4}{3h^2} F_{21}^{21} - \delta_A (M_{11}^{22} - \frac{4}{3h^2} N_{11}^{22})$$

$$b_6 = -R_{23}^{23} + \frac{4}{h^2} S_{23}^{23} = b_7$$

$$b_8 = -\delta_c (m_3 - \frac{4}{3h^2} m_5)$$

$$b_9 = -\delta_A \delta_B I_{33}^{22} - \delta_c \frac{4}{3h^2} m_5$$

$$c_1 = R_{13}^{13} - \frac{4}{h^2} S_{13}^{13}$$

$$c_2 = R_{23}^{23} - \frac{4}{h^2} S_{23}^{23}$$

$$c_3 = R_{13}^{13} - \frac{4}{h^2} S_{13}^{13} + T_{11}$$

$$c_4 = R_{23}^{23} - \frac{4}{h^2} S_{23}^{23} + T_{22}$$

$$c_5 = 1,\ c_6 = m_1$$

Here δ_A and δ_B are two tracers identifying the static and dynamic contributions of σ_{33}, respectively, whereas δ_c is a tracer identifying the effect of rotary inertia terms (see Refs. 13 and 14).

The coefficients in Eqs. (2) are

$$a_1 = 0;\ a_2 = 0;\ a_3 = D_{11}^{11};\ a_4 = D_{12}^{12};\ a_5 = D_{22}^{11} + D_{12}^{12};$$

$$a_6 = -K^2 R_{13}^{13};\ a_7 = -K^2 R_{13}^{13};\ a_8 = \delta_c m_3;\ a_9 = 0;$$

$$b_1 = 0;\ b_2 = 0;\ b_3 = D_{22}^{22};\ b_4 = D_{21}^{21};\ b_5 = D_{11}^{22} + D_{21}^{21};$$

$$b_6 = -K^2 R_{23}^{23};\ b_7 = -K^2 R_{23}^{23};\ b_8 = \delta_c m_3;\ b_9 = 0;$$

$$c_1 = K^2 R_{13}^{13};\ c_2 = K^2 R_{23}^{23};\ c_3 = K^2 R_{13}^{13} + T_{11};$$

$$c_4 = K^2 R_{23}^{23} + T_{22};\ c_5 = 1;\ \text{and}\ c_6 = m_1$$

In the above, D_{mn}^{ij}, F_{mn}^{ij}, . . . , R_{mn}^{ij} denote the rigidity components and $m_i (i = 1,3,5)$ are the reduced mass terms of the composite laminated plate defined in Refs. 13 and 14, and K^2 denotes the transverse shear correction factor.

Appendix B: The terms K_{ij} and $\bar{T}_i$ intervening in Equation 6

$$K_{11} = a_3 \alpha_m^2 + a_4 \beta_n^2 - a_6;\ K_{12} = a_5 \alpha_m \beta_n$$

$$K_{13} = a_1 \alpha_m^3 + a_2 \alpha_m \beta_n^2 - a_7 \alpha_m;\ K_{21} = b_5 \alpha_m \beta_n$$

$$K_{22} = b_4 \alpha_m^2 + b_3 \beta_n^2 - b_6;\ K_{23} = b_1 \beta_n^3 + b_2 \beta_n \alpha_m^2 - b_7 \beta_n$$

$$K_{31} = c_1 \alpha_m;\ K_{32} = c_2 \beta_n;\ K_{33} = c_3 \alpha_m^2 + c_4 \beta_n^2$$

$$\bar{T}_1 = sM_{11}^{(cs)}(m,n) + M_{12}^{(cs)}(m,n)$$

$$\bar{T}_2 = sM_{21}^{(sc)}(m,n) + M_{22}^{(sc)}(m,n)$$

$$\bar{T}_3 = sM_{31}^{(ss)}(m,n) + M_{32}^{(ss)}(m,n) + c_5 \bar{P}_z^{(ss)}(m,n,s)$$

where

$$M_{11}^{(cs)} = a_8 \bar{\psi}_x^{(cs)}(m,n) + a_9 \tilde{w}_x^{(cs)}(m,n)$$

$$M_{12}^{(cs)} = a_8 \tilde{\psi}_x^{(cs)}(m,n) + a_9 \tilde{\tilde{w}}_x^{(cs)}(m,n)$$

$$M_{21}^{(sc)} = b_8 \bar{\psi}_y^{(sc)}(m,n) + b_9 \tilde{w}_y^{(sc)}(m,n)$$

$$M_{22}^{(sc)} = b_8 \tilde{\psi}_y^{(sc)}(m,n) + b_9 \tilde{\tilde{w}}_y^{(sc)}(m,n)$$

$$M_{31}^{(ss)} = c_6 \tilde{W}_x^{(ss)}(m,n),\ \text{and}\ M_{32}^{(ss)} = c_6 \tilde{\tilde{w}}_y^{(ss)}(m,n)$$

Appendix C: The expression of the coefficients $I_{i,j,k}$ and λ_i

The coefficients I_{ijl} appearing in Eq. (11) are

$$I_{111} = b_8 c_6;\ I_{112} = -c_6 K_{22} - b_8 K_{33} + b_9 \beta_n K_{32}$$

$$I_{113} = K_{22} K_{33} - K_{32} K_{23};\ I_{121} = 0;\ I_{122} = c_6 K_{12} - a_9 \alpha_m K_{22}$$

$$I_{123} = K_{32} K_{13} - K_{12} K_{33};\ I_{131} = -a_9 b_8 \alpha_m$$

$$I_{132} = a_9 \alpha_m K_{22} - b_9 \beta_n K_{12} + b_8 K_{13};\ I_{133} = K_{12} K_{23} - K_{22} K_{13}$$

$$I_{211} = 0;\ I_{212} = c_6 K_{21} - b_9 \beta_n K_{31};\ I_{212} = K_{31} K_{23} - K_{21} K_{33}$$

$$I_{221} = a_8 c_6;\ I_{222} = -c_6 K_{11} - a_8 K_{33} + a_9 \alpha_m K_{31};$$

$$I_{223} = K_{11} K_{33} - K_{31} K_{13}$$

$$I_{231} = -a_8 b_9 \beta_n;\ I_{232} = -a_9 \alpha_m K_{21} + a_8 K_{23} + b_9 \beta_n K_{11}$$

$$I_{233} = K_{21} K_{13} - K_{11} K_{23};\ I_{311} = 0;\ I_{312} = b_8 K_{31};$$

$$I_{313} = K_{21} K_{32} - K_{22} K_{31}$$

$$I_{321} = 0;\ I_{322} = a_8 K_{32};\ I_{323} = K_{12} K_{31} - K_{32} K_{11}$$

$$I_{331} = a_8 b_8;\ I_{332} = -b_8 K_{11} - a_8 K_{22};\ I_{333} = K_{11} K_{22} - K_{12} K_{21}$$

The coefficients λ_i appearing in Eq. (11) are

$$\lambda_1 = a_8 b_8 c_6$$

$$\lambda_2 = K_{11} b_8 c_6 + K_{22} a_8 c_6 + K_{33} b_8 a_8 - K_{31} a_9 b_8 \alpha_m - K_{32} a_8 b_9 \beta_n$$

$$\lambda_3 = K_{11} K_{22} c_6 + K_{11} K_{33} b_8 + K_{22} K_{33} a_8 + K_{21} K_{32} a_9 \alpha_m + K_{31} K_{12} b_9 \beta_n - K_{11} K_{32} b_9 \beta_n - K_{32} K_{23} a_8 - K_{21} K_{12} c_6 - K_{31} K_{13} b_8 - K_{31} K_{22} a_9 \alpha_m$$

$$\lambda_4 = K_{11} K_{22} K_{33} + K_{21} K_{32} K_{13} + K_{31} K_{12} K_{23} - K_{11} K_{32} K_{23} - K_{22} K_{13} K_{31} - K_{33} K_{21} K_{12}$$

References

[1]Crocker, M. J., "Multimode Response of Panels to Normal and to Traveling Sonic Booms," *Journal of the Acoustical Society of America*, Vol. 42, 1967, p. 1070.

[2]Crocker, M. J. and Hudson, R. R., "Structural Response to Sonic Booms," *Journal of Sound and Vibrations*, Vol. 9, No. 3, 1969, pp. 454–468.

[3]Crocker, M. J., "Theoretical and Experimental Response of Panels to Traveling Sonic Boom and Blast Waves," Wyle Laboratories-Research Staff, Rept. WR 66-2, 1966.

[4]Cheng, D. H. and Benveniste, J. E., "Sonic Boom Effects on Structures—A Simplified Approach," *Trans. N.Y. Acad. Sci.*, Ser. II No. 30, 1968, pp. 457–478.

[5]Houlston, R., Slater, J. E., Pegg, N. and Des Rochers, C. G., "On the Analysis of Structural Response of Ship Panels Subjected to Air Blast Loading," *Computers of Structures*, Vol. 21, 1985, pp. 273–289.

[6]Rajamani A. and Prabhakaran, R., "Response of Composite Plates to Blast Loading," *Expl. Mech*, Vol. 20, 1980, pp. 245–250.

[7]Gupta, A. D., "Dynamic Analysis of a Flat Plate Subjected to an Explosive Blast," *Proceedings of the ASME International Computers Engineering Conference*, 1, 1985, pp. 491–496.

[8]Gupta, A. D., Gregory, F. H., and Bitting, R. L., "Dynamic Response of a Simply Supported Rectangular Plate to an Explosive Blast," *Proc. XIII Southeastern Conf. on Theoretical and Appl. Mech. 1*, 1985, pp. 385–390.

[9]Dobyns, A. L., "Analysis of Simply Supported Orthotropic Plates Subject to Static and Dynamic Loads," *AIAA Journal*, Vol. 19, 1981, pp. 642–650.

[10]Birman, V. and Bert, C. W., "Behavior of Laminated Plates Subjected to Conventional Blast," *International Journal of Impact Engineering*, Vol. 6, No. 3, 1987, pp. 145–155.

[11]Librescu, L., Khdeir, A. A., Reddy, J. N., "Further Results Concerning the Dynamic Response of Elastic Orthotropic Plates," *Zeitschrift für Angewandte Mathematik und Mechanik*, Vol. 69, 1989, p. 9.

[12]Gottlieb, J. J. and Ritzel, D. V., "Analytical Study of Sonic Boom From Supersonic Projectiles," *Progress in Aerospace Sciences*, Vol. 25, 1988, pp. 131–188.

[13]Librescu, L. and Khdeir, A. A., "Analysis of Symmetric Cross-Ply Laminated Elastic Plates Using a Higher Order Theory," *Composite Structures*, Part I, No. 7, 1988, pp. 189–213.

[14]Khdeir, A. A. and Librescu, L., "Analysis of Symmetric Cross-Ply Laminated Elastic Plates Using the Higher Order Theory," Part II, *Composite Structures*, No. 9, 1988, pp. 259–277.

[15]Cheng, D. H. and Benveniste, J. E., "Transient Response of Structural Elements to Traveling Pressure Waves of Arbitrary Shape," *International Journal of Mechanical Science*, Vol. 8, 1966, pp. 607–618.